

Magnetization Dynamics in Proximity-Coupled Superconductor-Ferromagnet-Superconductor Multilayers. II. Thickness Dependence of the Superconducting Torque

I.A. Golovchanskiy^{1,2,3,*}, N.N. Abramov,² O.V. Emelyanova,^{2,4,5} I.V. Shchetinin,² V.V. Ryazanov,^{1,2,6}
A.A. Golubov,^{1,7} and V.S. Stolyarov^{1,2,3}

¹ Moscow Institute of Physics and Technology, State University, 9 Institutskiy per., Dolgoprudny, Moscow Region 141700, Russia

² National University of Science and Technology MISIS, 4 Leninsky prosp., Moscow 119049, Russia

³ Dukhov Research Institute of Automatics (VNIIA), Moscow 127055, Russia

⁴ National Research Nuclear University MEPhI, Moscow 115409, Russia

⁵ Shubnikov Institute of Crystallography, Federal Scientific Research Centre “Crystallography and Photonics”, Russian Academy of Sciences, Moscow 119333, Russia

⁶ Institute of Solid State Physics (ISSP RAS), Chernogolovka, Moscow region 142432, Russia

⁷ Faculty of Science and Technology and MESA+ Institute for Nanotechnology, University of Twente, Enschede 7500 AE, Netherlands



(Received 5 August 2022; revised 2 December 2022; accepted 1 February 2023; published 8 March 2023)

In this work, we study magnetization dynamics in superconductor-ferromagnet-superconductor thin-film structures. Results of the broad-band ferromagnetic resonance spectroscopy are reported for a large set of samples with varied thickness of both superconducting and ferromagnetic layers in a wide frequency, field, and temperature ranges. Experimentally the one-dimensional anisotropic action of superconducting torque on magnetization dynamics is established; its dependence on thickness of layers is revealed. It is demonstrated that experimental findings support the recently proposed mechanism of the superconducting torque formation via the interplay between the superconducting imaginary conductance and magnetization precession at superconductor-ferromagnet interfaces. Microwave spectroscopy studies in this work are supplemented by investigations of the crystal structure and the microstructure of studied multilayers.

DOI: 10.1103/PhysRevApplied.19.034025

I. INTRODUCTION

Advantages from hybridization of antagonistic superconducting and ferromagnetic orders in electronics and spintronics have been repeatedly demonstrated in past decades [1]. The interplay between ferromagnetic and superconducting spin orders enables manipulation with spin states and leads to the development of various electronic and spintronic elements, including superconductor-ferromagnet-superconductor (*S-F-S*) Josephson junctions [1–3], superconducting phase shifters [4,5], memory elements [6–8], *F-S-F*-based spin valves [9,10], Josephson diodes [11], and more complex long-range spin-triplet superconducting systems [12–16].

Recently, the application capabilities of *S-F* hybridization have been expanded by demonstrations of its prospects in magnonics. Magnonics is a growing field of research, which offers approaches for the transfer and processing of information via spin waves. For

instance, conventional magnonics is progressed towards the development of magnon logic devices and circuit elements, such as waveguides [17], transistors [18], majority gates [19,20], and other elements. As an alternative, cavity magnonics [21] considers hybridization of magnons with photons and aims at the single quantum operations [22,23]. A good overview of various potential applications and recent advances in magnonics can be found in Refs. [24–31] and references therein. In the development of magnonic systems one of the principle requirements is engineering of appropriate spin-wave dispersion and its tunability.

Various wide-range manipulations with the spin-wave dispersion have been demonstrated at cryogenic temperatures when coupling magnonic systems with superconductors. For instance, interaction of a magnonic media with the superconducting vortex matter allows the formation and tuning of forbidden bands at submicrometer wavelength, which matches the parameter of the vortex lattice [32], or excitation of exchange spin waves via driving the vortex lattice with the electric current [33]. Also, magnetostatic

*Corresponding author. golov4anskiy@gmail.com

interaction of spin waves with superconducting Meissner currents in thin-film hybrid structures modifies substantially the spin-wave dispersion [34,35] and can be used to form magnonic crystals [36] or to gate the magnon current [37]. Remarkably, low speed of electromagnetic propagation in superconductor-insulator-superconductor thin-film structures facilitates achievement of the ultrastrong photon-to-magnon coupling in on-chip hybrid devices [38,39].

A striking phenomenon in *S-F* hybrid structures was discovered recently in Ref. [40] using three-dimensional (3D) cavity resonance spectroscopy, confirmed in Ref. [41] using the same technique, and studied experimentally in more details in Ref. [42] using the broad-band ferromagnetic resonance (FMR) spectroscopy. In superconductor-ferromagnet-superconductor trilayer thin-film structures a radical increase in the FMR frequency occurs in the presence of electronic interaction between superconducting and ferromagnetic layers. The phenomenon is strong: in some *S-F-S* structures the highest natural FMR frequencies are reached among in-plane magnetized ferromagnetic systems [42]. In addition, the broad-band FMR [42] reveals nontrivial effect of the electronic interaction between superconducting and ferromagnetic layers on magnetic anisotropies.

Intriguingly, while a few different mechanisms have been proposed for explanation of the phenomenon [40,41,43], these proposals lack consistency with experimental results. In particular, the originally proposed mechanism [40] suggests involvement of spin-triplet superconducting correlations, which is inconsistent with typical frequencies of the phenomena as well as with rather large thicknesses of ferromagnetic layers [42]. Another proposed mechanism suggests involvement of the superconducting vortex phase [41] and disagrees with the thickness dependence of the phenomenon as well as with several other circumstantial factors [42]. At last, a magnetostatic mechanism proposed in Ref. [43], as it appears, predicts different from the experiment dependence of the phenomenon on thickness of ferromagnetic layer. Thus, the mechanism behind the phenomenon remains unestablished.

In this work, we report a comprehensive experimental study of the phenomenon. We report results of FMR spectroscopy for a large set of samples with varied thickness of both superconducting and ferromagnetic layers in a wide frequency, field, and temperature ranges. We establish an anisotropic one-dimensional action of hybridization-induced torque acting on magnetization dynamics and the dependence of this superconducting torque on the magnetic field. Experimental results support the recently proposed model by Silaev [44], which explains the phenomenon in *S-F-S* structures as the outcome of the coupling between magnetization dynamics and superconducting imaginary conductance at *S-F* interfaces.

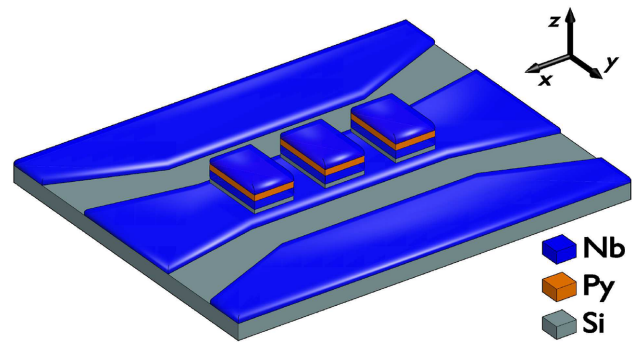


FIG. 1. Schematic illustration of the investigated chip-sample (adopted from Ref. [42]). A series of *S-F-S* film rectangles is placed directly on top of the central transmission line of niobium co-planar waveguide. Magnetic field H is applied in-plane along the x -axis.

II. EXPERIMENTAL DETAILS

Magnetization dynamics in *S-F-S* structures is studied by measuring the ferromagnetic resonance absorption spectrum using the so-called VNA-FMR approach [45–48], where VNA stands for the vector network analyzer. A schematic illustration of investigated samples is shown in Fig. 1. The chip consists of a thin-film superconducting niobium (Nb) co-planar waveguide with 50-Ohm impedance and 82-150-82 μm gap-center-gap dimensions and a series of niobium-permalloy($\text{Py}=\text{Fe}_{20}\text{Ni}_{80}$)-niobium (Nb-Py-Nb) film structures with lateral dimensions $X \times Y = 50 \times 140 \mu\text{m}$ and spacing of 25 μm along the x axis that are placed directly on top of the central transmission line of the waveguide. Deposition of Nb-Py-Nb trilayers is performed in a single vacuum cycle ensuring the electron transparency at Nb-Py interfaces. Thin Si or AlO_x spacing layer is deposited between Nb co-planar waveguide and the trilayers in order to ensure electrical insulation of the studied samples from the waveguide. As a result, a series of samples has been fabricated and measured with different thickness of superconducting (*S*) and ferromagnetic (*F*) layers (see Table I).

General crystal structure of as-fabricated samples is studied with the x-ray diffraction (XRD) using Rigaku Ultima IV diffractometer equipped with $\text{Cu-K}\alpha$ -source and graphite monochromator. Local crystal microstructure and elemental composition are studied via TEM. Cross-section lamellas from chip samples for TEM investigations are prepared by focused ion-beam system integrated in dual beam scanning electron microscope Helios G4 Plasma FIB Uxe. Bright-field (BF) images, selected-area electron-diffraction (SAED) patterns, high-angle annular dark-field scanning transmission electron microscopy (HAADF STEM) images and energy dispersive x-ray (STEM EDX) compositional maps are collected on a probe aberration-corrected FEI Titan Themis Z electron microscope at 200 kV equipped with a Super-X system for EDX analysis.

TABLE I. Parameters of studied samples. The d_s and d_F denote thickness of superconducting and ferromagnetic layers, respectively. Parameters H_a and M_{eff} are obtained by fitting resonance lines at $T > T_c$ with Eq. (1) and are temperature independent. Parameters H_{s0} , T_c , and p are obtained first by fitting resonance lines at $T < T_c$ with Eq. (2) using fixed parameters H_a and M_{eff} , and next by fitting $H_s(T)$ in Fig. 7 with Eq. (3).

Sample ID	d_s (Nb), nm	d_F (Py), nm	d_s (Nb), nm	$\mu_0 H_a$, mT	$\mu_0 M_{\text{eff}}$, T	$\mu_0 H_{s0}$, mT	T_c , K	p
S1	110	10	110	1.5	1.051	31.8	8.74	3.79
S2	120	11	120	-3.3	1.029	39.1	8.56	3.70
S3	110	19	110	-0.15	1.100	78.8	8.90	3.48
S4	100	35	100	-0.2	1.132	163.6	8.92	3.80
S5	140	45	174	-0.4	1.18	193.7	9.08	4.90
S6	110	120	110	-0.1	1.123	352.6	8.82	4.56
S7	110	350	110	1.6	1.076	617.2	8.74	8.89
S8	41	24	41	-0.2	1.131	37.8	7.51	3.07
S9	200	30	50	-1	1.146	96.8	8.74	4.38

Microwave spectroscopy of samples is performed by measuring the transmission characteristics $S_{21}(f', H)$ in the closed-cycle cryostat Oxford Instruments Triton (base temperature 1.2 K) equipped with the home-made superconducting solenoid. Spectroscopy is performed in the field range from -0.22 T to 0.22 T, in the frequency range from 0 up to 20 GHz, and in the temperature range from 2 to 11 K. Magnetic field is applied in plane along the direction of the waveguide in Fig. 1. FMR spectra at different temperatures are analyzed by fitting $S_{21}(f')$ characteristics at specified H and T with the Lorentz curve and, thus, obtaining the dependencies of the resonance frequency on magnetic field $f_r(H)$.

III. STRUCTURE CHARACTERIZATION

Microstructure and the crystal structure of fabricated samples is characterized using the S6 sample as the representative example. Figure 2 shows the x-ray diffraction pattern of the S6 sample. Apart from the(001)-type lines of the Si substrate the pattern contains only rather wide (110)-type reflexes of niobium and (111)-type reflexes of

permalloy. Such an XRD pattern indicates a highly textured crystal structure of deposited films with the growth direction being the crystal dense packing direction.

The typical BF TEM image and SAED diffraction patterns for a cross-section chip sample are given in Figs. 3(a)–3(c), respectively, and demonstrate the overall morphological characteristics of the multilayered chip sample. BF TEM image [Fig. 3(a)] indicates rather sharp Nb-Py interfaces with the peak-to-peak roughness not exceeding about 4 nm. Also, polycrystalline columnar grain structure is clearly visible in Nb and Py layers. The major part of grain boundaries is found to be perpendicular to the film surfaces and interfaces. The grain size is equal to the film thickness in growth direction while it varies from 10 to 40 nm in lateral direction. The SAED patterns of Nb and Py [Figs. 3(b) and 3(c)] are composed of a series of Debye-Scherrer rings and lines of strong diffraction spots (marked by arrows) parallel to the film growth directions. The absence of diffuse intensity rings (halo type) in SAED patterns confirms the crystalline nature of Nb and Py layers. Lines of diffraction spots correspond to (110) and (111) crystallographic planes of Nb and permalloy layers,

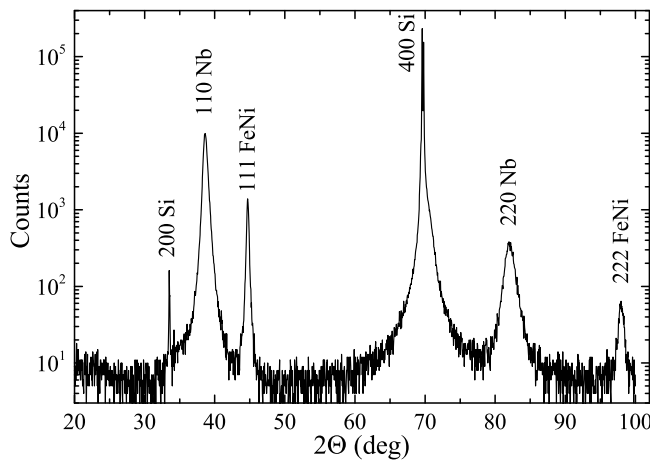


FIG. 2. XRD spectrum of the S6 sample with identified lines.

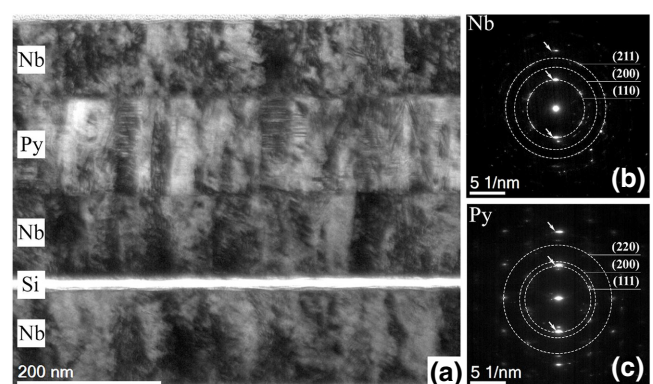


FIG. 3. (a) BF TEM image of the cross section of multilayered chip sample. (b),(c) Typical SAED patterns of niobium (b) and permalloy (c) layers.

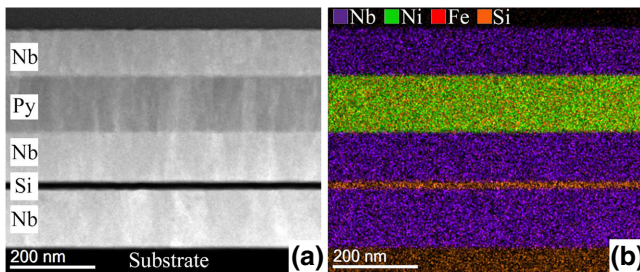


FIG. 4. (a) HAADF STEM image of the area used for the elemental mapping. (b) Color-coded STEM EDX elemental map.

respectively, in consistency with XRD studies (Fig. 2). Obtained SAED patterns indicate that both layers consist of strongly textured crystalline grain ensembles with the random out-of-plane orientation and in-plane orientation (110)-Nb and (111)-Py growth direction.

The STEM EDX compositional map of the chip sample is shown in Fig. 4. It demonstrates a homogeneous distribution of Ni and Fe within the permalloy layer as well as no interdiffusion, impurity segregation or visible precipitates.

In order to confirm the absence of noticeable intermixing between layers an elemental distribution profile across the Nb-permalloy interface is provided in Fig. 5. Elemental profile confirms the homogeneity of elemental distribution within the individual layers. The elemental content of the permalloy layer corresponds to the nominal composition. The transient layer with the thickness of 7.6 nm can be distinguished at the Nb-permalloy interface, which is attributed to unsharp morphology of the interface.

IV. MICROWAVE SPECTROSCOPY RESULTS

Figure 6 demonstrates the essence of the studied phenomenon for the S4 sample (see Table I), which is used

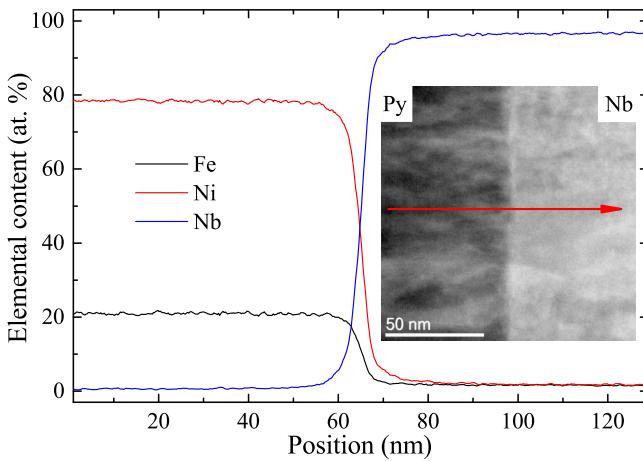


FIG. 5. STEM EDX elemental distribution profile across the Nb-permalloy interface extracted along the arrow overplotted on the HAADF STEM image in the inset.

as the representative example. The S4 sample consists of 100-nm-thick Nb layers and 35-nm-thick Py layer. Figures 6(a) and 6(b) show, correspondingly, transmission spectra at temperatures well below the superconducting critical temperature of Nb ($T_c \approx 9$ K) and above T_c . Both spectra contain a single-resonance absorption line and demonstrate that at temperatures below T_c the resonance line is observed at radically higher frequencies. Some interruptions of resonance lines in Figs. 6(a) and 6(b) appear due to the parasitic box mode resonances in the sample holder. Figure 6(c) illustrates cross sections of transmission spectra at $\mu_0 H = 20$ mT and selected temperatures. Figure 6(d) collects dependencies of the FMR frequency on magnetic field $f_r(H)$ and shows that upon decreasing the temperature below T_c the resonance curve $f_r(H)$ shifts gradually to higher frequencies. For instance, upon decreasing the temperature the frequency of the natural FMR $f_r(H = 0)$ increases from about 0.5 GHz at $T \geq 9$ K to about 13 GHz at $T = 2$ K.

At $T > T_c$ FMR curves $f_r(H)$ in Figs. 6(b) and 6(d) follow the typical Kittel dependence for thin in-plane-magnetized ferromagnetic films at in-plane magnetic field:

$$(2\pi f_r/\mu_0\gamma)^2 = (H + H_a)(H + H_a + M_{\text{eff}}), \quad (1)$$

where μ_0 is the vacuum permeability, $\gamma = 1.856 \times 10^{11}$ Hz/T is the gyromagnetic ratio for permalloy, H_a is the uniaxial anisotropy field that is aligned with the external field, and M_{eff} is the effective magnetization, which includes the saturation magnetization M_s and the out-of-plane anisotropy field. For all studied samples the fit of FMR curves obtained in the temperature range $T = 9 - 11$ K $> T_c$ with Eq. (1) yields negligible anisotropy field H_a , the effective magnetization $M_{\text{eff}} \approx 1.0 - 1.2$ T, which is close to typical values of the saturation magnetization of permalloy $\mu_0 M_s \approx 1$ T, and no dependence of H_a and M_{eff} on temperature. Magnetic parameters H_a and M_{eff} for all studied samples are provided in Table I. The fit of $f_r(H)$ curves for the S4 sample with Eq. (1) at temperature $T = 9.5$ K $> T_c$ is shown in Fig. 6(d) with the yellow solid line.

At $T < T_c$ FMR curves obey a different expression. In Refs. [38,42] it was shown that technically by fitting $f_r(H)$ at $T \ll T_c$ with Eq. (1) the action of superconductivity results in equal but different in sign uniaxial anisotropy field H_a and changes of the effective magnetization ΔM_{eff} : $H_a \approx -\Delta M_{\text{eff}}$. Following the basics of derivation of the Kittel formula [49], this equality indicates that superconductivity acts on magnetization as the one-dimensional restoring torque along the y axis in Fig. 1, and the fitting function should take the form $f_r^2 \sim (H + H_s)(H + M_{\text{eff}})$, where H_s is the field of the superconducting torque. A satisfactory fit with such an expression can be obtained for all samples in Table I at temperatures $T \ll T_c$, while for the sample S8, which is based on thin superconducting layers

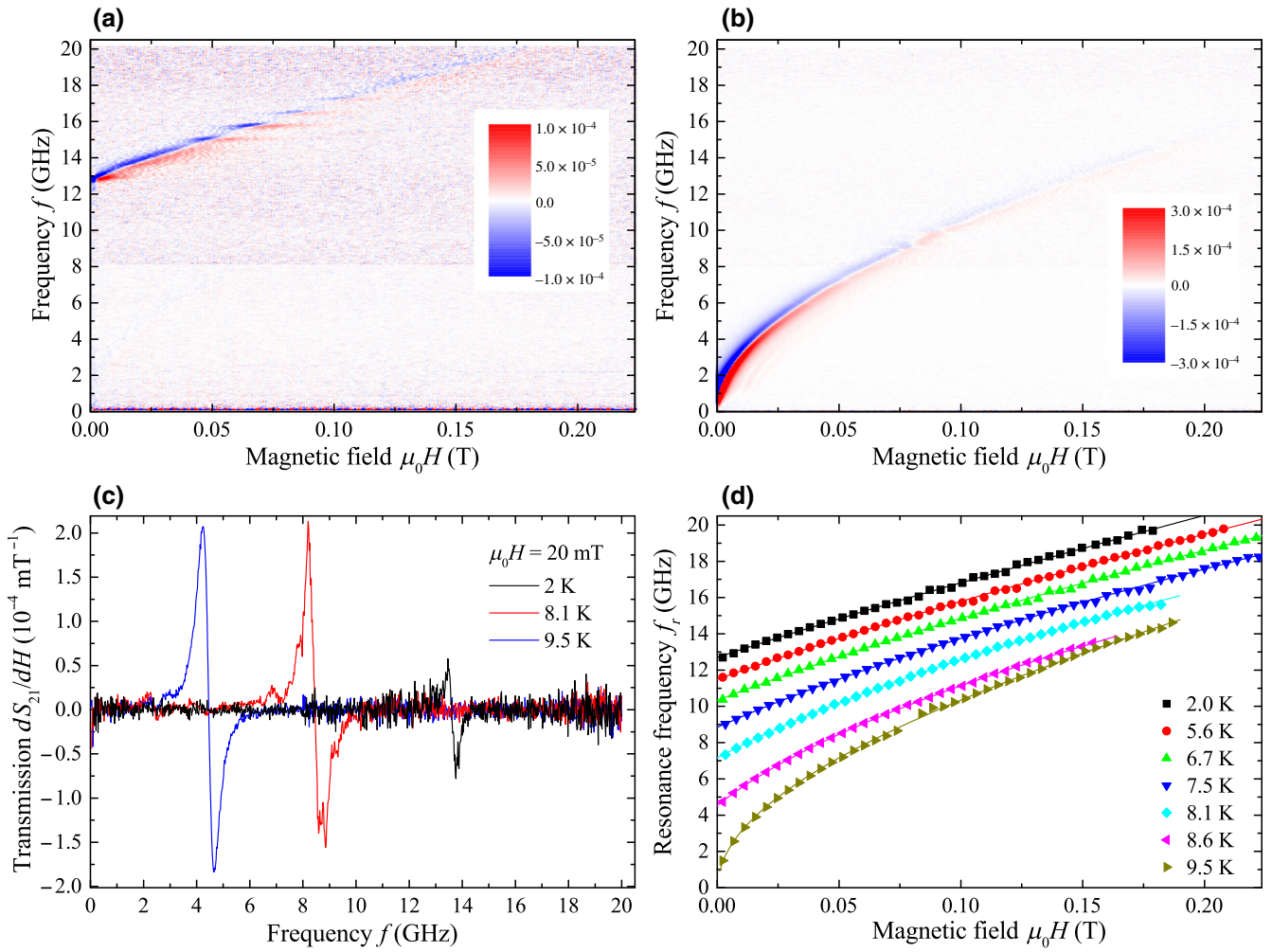


FIG. 6. (a),(b) Differentiated transmission spectra $dS_{21}/dH(f, H)$ at temperatures 2 K (a) and 9.5 K (b). Color codes are provided in spectra. (c) Cross section of transmission spectra $dS_{21}/dH(f')$ at magnetic field $\mu_0 H = 20$ mT and corresponding temperatures. (d) Symbols show experimental dependencies of the FMR frequency on magnetic field $f_r(H)$ for the S4 sample at different temperatures. Solid lines show corresponding fit of $f_r(H)$ dependencies with Eq. (1) at $T > T_c$ and with Eq. (2) at $T < T_c$.

with $d_s < \lambda_L$, this expression is valid in the entire temperature range. Here $\lambda_L \approx 80$ nm [38,50] is the London penetration depth in bulk niobium at zero temperature

However, as was also shown in Refs. [38,42] at temperatures $T \lesssim T_c$ the superconductivity-induced uniaxial anisotropy field H_a in Eq. (1) no longer corresponds to $-\Delta M_{\text{eff}}$. As it appears, this discrepancy is a rather artificial effect and can be explained by suppression of the superconducting torque upon increasing the magnetic field. In general, suppression of superconductivity by the applied field results in reduction of the critical temperature or in an increase in superconducting penetration depth [50]. At higher fields, suppression of the field H_s results in reduction of the derivative from the $f_r(H)$ curve. The fit of such a resonance line with the conventional Kittel formula [Eq. (1)] results in a larger reduction of the effective magnetization in comparison to the induced anisotropy $H_a < -\Delta M_{\text{eff}}$ at temperatures $T \lesssim T_c$. We find that at $T < T_c$

FMR curves $f_r(H)$ for all studied samples in Table I obey the modified Kittel dependence:

$$(2\pi f_r/\mu_0\gamma)^2 = (H + H_a + H_s(1 - \alpha_s H^2)) \times (H + H_a + M_{\text{eff}}), \quad (2)$$

where H_a and M_{eff} are constants and are derived at $T > T_c$ (see Table I), H_s is the field of one-dimensional superconducting torque at zero applied field, and the parameter α_s reflects the dependence of the superconducting torque on applied magnetic field. We confirm that for all studied samples, FMR curves at all temperatures $T < T_c$ can be fitted with Eq. (2). Examples of such a fit are shown for the S4 sample in Fig. 6(d) with solid lines.

Analysis of resonance lines $f_r(H)$ with Eqs. (1) and (2) yields dependencies of the superconducting torque field and of the field-dependence coefficient on temperature, $H_s(T)$ and $\alpha_s(T)$. This data is provided for all studied

samples in Figs. 7(a)–7(c). Notice that for all samples except S8 and S7 the parameter α_s growth exponentially from $\alpha_s \sim 1 \text{ T}^{-2}$ at $T \approx 6 \text{ K}$ up to $\alpha_s \sim 10^2 \text{ T}^{-2}$ at $T \approx 8.5 \text{ K}$. The range of temperatures where the suppression of the superconducting torque field by the applied field is insignificant can be derived from Fig. 7(c) and the condition $\alpha_s H^2 \ll 1$. For instance, for all studied samples in the studied field range $\mu_0 H < 0.23 \text{ T}$ the suppression is insignificant at $T < 5 \text{ K}$.

Temperature dependence of the torque field $H_s(T)$ can be characterized by fitting it with the following expression [42]:

$$H_s = H_{s0} (1 - (T/T_c)^p), \quad (3)$$

where H_{s0} is the superconducting spin-torque field at zero field and zero temperature, T_c is the superconducting critical temperature of *S*-*F*-*S* trilayers, and p is a free exponent parameter. The fit of $H_s(T)$ with Eq. (3) for all samples is shown in Figs. 7(a) and 7(b) with solid lines and yields parameters H_{s0} and p provided in Table I. Notice that for all samples, except S7, which contains the the thickest *F* layer, the exponent p is in the range from about 3 up to 5 with the average value of about 4. Also we notice that due to technical limitations, resonance curves of the S7 sample with the thickest *F* layer could be measured only above 8 K and the value of H_s below 8 K is obtained via the extrapolation with Eq. (3). This extrapolation yields the natural FMR frequency in the S7 sample $f_r(H = 0) = 24.1 \text{ GHz}$ at zero temperature in the case if the value $p = 8.89$ is

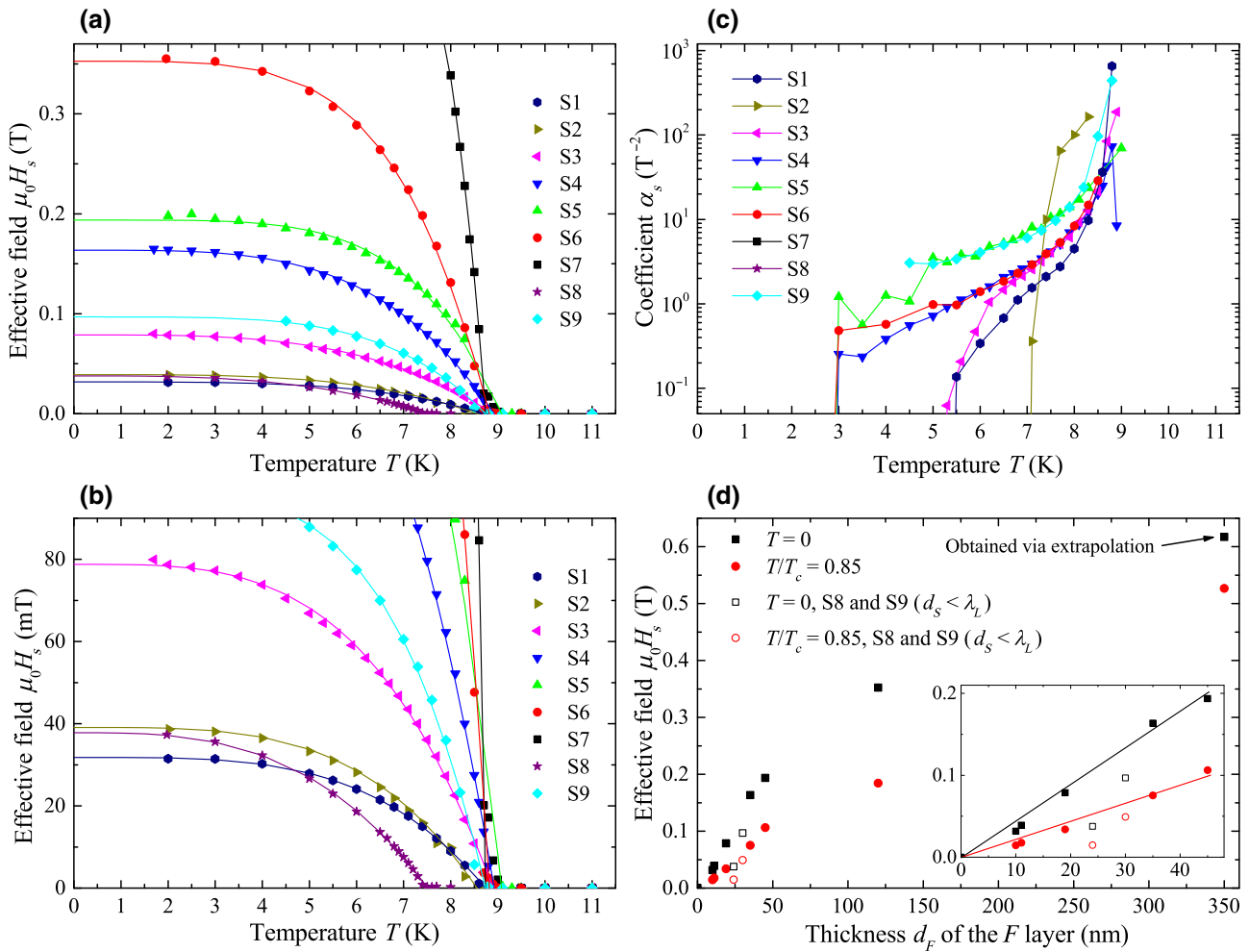


FIG. 7. (a) Dependencies of the superconducting torque field on temperature $H_s(T)$ at zero external field. (b) Magnification of (a) at $\mu_0 H_s < 0.1 \text{ T}$. Solid lines in (a),(b) show the fit of experimental $H_s(T)$ curves with Eq. (3). (c) Dependencies of the field-dependence coefficient of the superconducting torque field in Eq. (2) on temperature $\alpha_s(T)$. (d) The dependence of the superconducting torque field on the thickness of ferromagnetic layer $H_s(d_F)$ at zero field at $T = 0$ (black symbols) and at $T/T_c = 0.85$ red symbols. Solid symbols represent data for samples with both superconducting layers $d_s > \lambda_L$. Open symbols represent data for two samples (S8 and S9) with $d_s < \lambda_L$ at least for one superconducting layer. See Table I for details. The inset in (d) magnifies $H_s(d_F)$ for $d_F < 45 \text{ nm}$. Solid lines in the inset in (d) show the linear fit of $H_s(d_F)$ at corresponding temperature.

correct, or $f_r(H = 0) = 30.0$ GHz for $p = 4.9$ (in the latter case $\mu_0 H_{s0} = 0.96$ T), which is the maximum value observed among the rest of the samples in Table I.

Figure 7(d) shows the dependence of the superconducting torque field on the thickness of ferromagnetic layer $H_s(d_F)$ at zero temperature [i.e., parameter H_{s0} in Eq. (3)] and at $T/T_c = 0.85$. This is the core result of this work. Figure 7(d) clearly demonstrates the overall logarithmic-like dependence of H_s on thickness d_F , with the linear growth of H_s at low d_F [see the inset in Fig. 7(d)] and retardation of H_s growth at higher d_F . Also, Fig. 7(d) reveals the dependence of the superconducting torque field on the thickness of superconducting layers: in this case the thickness of one of the S layers is reduced and H_s is also reduced [open symbols in Fig. 7(d)]. Notice that while in the case of the S8 sample this reduction can be partially explained by suppressed superconductivity and smaller $T_c \approx 7.5$ K, this is not the case for the S9 sample where T_c is comparable with values for the rest of the samples.

V. DISCUSSION

The original explanation [40] of the phenomenon in S - F - S trilayers suggested the role of spin-polarized spin-triplet Cooper pairs in the formation of the superconductivity-induced anisotropy via the spin-transfer-torque mechanism. Yet, this mechanism requires the frequency of magnetization dynamics comparable with the depairing frequency of the superconducting gap [51], requires superconducting coherence across the F layer, which can hardly be expected for 120-nm or 350-nm-thick junctions even in the case of spin-triplet pairs, and does not yield the one-dimensional torque on magnetic moment. Later the role of superconducting vortices was suggested [41], which however is inconsistent with experimental results in quite a number of ways [42], including the fact of the absence of the effect in S - F - I - S structures. It should be noted that earlier works [40,41] used 3D cavity resonators for spectroscopy, which provide a single resonance field point at the resonance frequency of the cavity instead of the entire FMR curve as in broad-band techniques, and thus, deviation of the FMR line from the conventional Kittel formula [Eq. (1)] in these works simply could not be detected.

The first hint on inductive origin of the phenomenon in S - F - S trilayers was reported in Ref. [43] where the magnetostatic interaction has been considered between the screening currents induced by ferromagnetic stray fields in S layers and the magnetic moment in the F layer. While only the static case is considered, it is shown that in the case where the superconducting currents are allowed to loop around the ferromagnetic layer, additional dc demagnetising field is expected with the following dependence

on magnetic and structural characteristics of trilayers:

$$H_s \propto M_s \frac{d_F}{\lambda_L} \frac{d_F}{L} \ln \frac{2L}{d_F}, \quad (4)$$

where L is the length of the structure. The theory in Ref. [43] provides an explanation for the one dimensionality of the demagnetizing field along the y axis in Fig. 1 and predicts the growth of the demagnetizing field with increasing thickness of the F layer. Yet, according to Eq. (4) this theory predicts a parabolic dependence of $H_s(d_F)$, which is inconsistent with Fig. 7(d), and some dependence of H_s on the length of the structure, which is not observed experimentally. In fact, this theory leads to a rather counterintuitive outcome that the effect in S - F - S structures where superconducting currents are allowed to loop around the ferromagnetic layer should be measurable with conventional magnetization measurements.

The mechanism behind the superconducting torque in S - F - S trilayers is revealed in Ref. [44]. The mechanism is purely electromagnetic and implies the coupling of the superconducting imaginary conductance in the S layer [52,53] with the precessing magnetization of the F layer at S - F interfaces. This electromagnetic interaction results in formation of macroscopic circulation currents curling around the y axis in the opposite phase with precessing magnetization (see Fig. 8). The model in Ref. [44] predicts exactly the same dependence of the resonance frequency on the magnetic field as in Eq. (2) in the limit $d_F \ll \lambda$:

$$H_s(1 - \alpha_s H^2) = M_s \frac{d_F}{2\lambda_L} \tanh \frac{d_S}{\lambda_L}. \quad (5)$$

In fact, Eq. (5) demonstrates the linear dependence of the superconducting torque on thickness d_F at small d_F , which is consistent with Fig. 7(d). The reduction of the superconducting torque upon increasing the magnetic field in Eq. (5) appears due to increase of the penetration depth

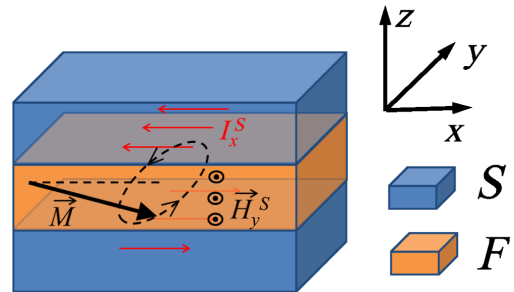


FIG. 8. Schematic illustration of the mechanism behind the superconducting torque in S - F - S trilayers [44]. Magnetization precession (\vec{M} , black arrow) at the S - F interface induces macroscopic superconducting currents circulating in S layers along the x direction (I_x^S , red arrows). These currents induce magnetic field H_y^S in y direction in the opposite phase to the precession of \vec{M} .

[50]: $(1 - \alpha_s H^2) \propto 1/\lambda_L(H) \tanh d_S/\lambda_L(H)$. The dependence of the superconducting torque on the thickness d_S of S layers is also captured in Eq. (5) as $\propto \tanh d_S/\lambda$. Both effects are observed in Fig. 7(d). At $d_F \gg \lambda$ the model in Ref. [44] predicts the saturation of the superconducting torque to a constant value $H_s \approx M_s$, which is also observed in Fig. 7(d). Thus, the role of superconducting imaginary conductance behind the dramatic increase of the FMR frequency in S - F - S trilayers with electronic interaction at S - F interfaces is confirmed.

As a final remark, it can be expected that superconductivity in S - F - S structures modifies the dispersion of perpendicular standing spin waves (PSSWs) [54–58]. In the case of closed PSSW boundary conditions [54,55,57] magnetization precession at both S-F interfaces does not take place and, thus, the superconducting torque is not formed. In the case of free PSSW boundary conditions [56,58] magnetization at S-F interfaces precesses at opposite phases for even modes and precesses in phase for odd modes, which corresponds to cancellation of the superconducting torque for even modes and its presence for odd modes, respectively. In the general case when the F layers are magnetically nonuniform across its thickness [58] and the spin boundary conditions are affected by surface anisotropies [59,60], the effect of the superconducting torque on the dispersion of PSSWs becomes nontrivial.

VI. CONCLUSION

Summarizing, we report a comprehensive experimental study of magnetization dynamics in S - F - S trilayers. We report results of FMR spectroscopy for a large set of samples with varied thicknesses of both superconducting and ferromagnetic layers in a wide frequency, field, and temperature ranges. Experimentally we establish an anisotropic one-dimensional action of hybridization-induced torque acting on magnetization dynamics and the dependence of this superconducting torque on the magnetic field. Experimental results confirm the recently proposed model by Silaev [44], which explains the phenomenon in S - F - S structures as the outcome of the coupling between magnetization dynamics and superconducting imaginary conductance at S - F interfaces. Our results open wide prospects for application of the superconductivity in magnonics. In addition, as was suggested in Ref. [44], S - F - S systems provide the playground for Anderson-Higgs mass generation of boson quasiparticles in high-energy Standard Model and in condensed-matter systems.

ACKNOWLEDGMENTS

The authors acknowledge Dr M. Silaev for fruitful discussions, critical reading of the paper and useful suggestions. The research study is financially supported by

the Russian Science Foundation (Grant No. 22-22-00314). Access to the TEM facilities is granted by Advance Imaging Core Facility of Skoltech.

- [1] J. Linder and J. W. A. Robinson, Superconducting spintronics, *Nat. Phys.* **11**, 307 (2015).
- [2] V. V. Ryazanov, V. A. Oboznov, A. Y. Rusanov, A. V. Veretennikov, A. A. Golubov, and J. Aarts, Coupling of Two Superconductors Through a Ferromagnet: Evidence for a π Junction, *Phys. Rev. Lett.* **86**, 2427 (2001).
- [3] M. Weides, M. Kemmler, E. Goldobin, D. Koelle, R. Kleiner, H. Kohlstedt, and A. Buzdin, Magnetic anisotropy in ferromagnetic Josephson junctions, *Appl. Phys. Lett.* **89**, 122511 (2007).
- [4] T. Yamashita, S. Kim, H. Kato, W. Qiu, K. Semba, A. Fujimaki, and H. Terai, π -phase shifter based on NbN-based ferromagnetic Josephson junction on a silicon substrate, *Sci. Rep.* **10**, 13687 (2020).
- [5] A. K. Feofanov, V. A. Oboznov, V. V. Bolginov, J. Lisenfeld, S. Poletto, V. V. Ryazanov, A. N. Rossolenko, M. Khabipov, D. Balashov, A. B. Zorin, P. N. Dmitriev, V. P. Koshelets, and A. V. Ustinov, Implementation of superconductor/ferromagnet/superconductor pi-shifters in superconducting digital and quantum circuits, *Nat. Phys.* **6**, 593 (2010).
- [6] I. A. Golovchanskiy, V. V. Bolginov, V. S. Stolyarov, N. N. Abramov, A. B. Hamida, O. V. Emelyanova, B. S. Stolyarov, M. Y. Kupriyanov, A. A. Golubov, and V. V. Ryazanov, Micromagnetic modeling of critical current oscillations in magnetic Josephson junctions, *Phys. Rev. B* **94**, 214514 (2016).
- [7] I. V. Vernik, V. V. Bol'ginov, S. V. Bakurskiy, A. A. Golubov, M. Y. Kupriyanov, V. V. Ryazanov, and O. Mukhanov, Magnetic Josephson junctions with superconducting interlayer for cryogenic memory, *IEEE Trans. Appl. Supercond.* **23**, 1701208 (2013).
- [8] L. N. Karelina, R. A. Hovhannisan, I. A. Golovchanskiy, V. I. Chichkov, A. B. Hamida, V. S. Stolyarov, L. S. Uspenskaya, S. A. Erkenov, V. V. Bolginov, and V. V. Ryazanov, Scalable memory elements based on rectangular SIsFS junctions, *J. Appl. Phys.* **130**, 173901 (2021).
- [9] E. C. Gingrich, B. M. Niedzielski, J. A. Glick, Y. Wang, D. L. Miller, R. Loloe, W. P. P. Jr, and N. O. Birge, Controllable 0- π Josephson junctions containing a ferromagnetic spin valve, *Nat. Phys.* **12**, 564 (2016).
- [10] D. Lenk, R. Morari, V. I. Zdravkov, A. Ullrich, Y. Khaydukov, G. Obermeier, C. Muller, A. S. Sidorenko, H.-A. K. von Nidda, S. Horn, L. R. Tagirov, and R. Tidecks, Full-switching FSF-type superconducting spin-triplet magnetic random access memory element, *Phys. Rev. B* **96**, 184521 (2017).
- [11] K.-R. Jeon, J.-K. Kim, J. Yoon, J.-C. Jeon, H. Han, A. Cottet, T. Kontos, and S. S. P. Parkin, Zero-field polarity-reversible Josephson supercurrent diodes enabled by a proximity-magnetized Pt barrier, *Nat. Mater.* **21**, 1008 (2022).
- [12] J. W. A. Robinson, J. D. S. Witt, and M. G. Blamire, Controlled injection of spin-triplet supercurrents into a strong ferromagnet, *Science* **329**, 59 (2010).

- [13] N. Banerjee, J. Robinson, and M. Blamire, Reversible control of spin-polarized supercurrents in ferromagnetic Josephson junctions, *Nat. Commun.* **5**, 4771 (2014).
- [14] J. Wang, M. Singh, M. Tian, N. Kumar, B. Liu, C. Shi, J. K. Jain, N. Samarth, T. E. Mallouk, and M. H. W. Chan, Interplay between superconductivity and ferromagnetism in crystalline nanowires, *Nat. Phys.* **6**, 389 (2010).
- [15] J. A. Glick, V. Aguilar, A. Gougam, B. M. Niedzielski, E. C. Gingrich, R. Loloei, W. P. P. Jr., and N. O. Birge, Phase control in a spin-triplet SQUID, *Sci. Adv.* **4**, eaat9457 (2020).
- [16] K.-R. Jeon, B. K. Hazra, K. Cho, A. Chakraborty, J.-C. Jeon, H. Han, H. L. Meyerheim, T. Kontos, and S. S. P. Parkin, Long-range supercurrents through a chiral non-collinear antiferromagnet in lateral Josephson junctions, *Nat. Mater.* **20**, 1358 (2021).
- [17] P. Wessels, A. Vogel, J.-N. Tödt, M. Wieland, G. Meier, and M. Drescher, Direct observation of isolated Damon-Eshbach and backward volume spin-wave packets in ferromagnetic microstripes, *Sci. Rep.* **6**, 22117 (2016).
- [18] A. V. Chumak, A. A. Serga, and B. Hillebrands, Magnon transistor for all-magnon data processing, *Nat. Commun.* **5**, 4700 (2014).
- [19] K. Ganzhorn, S. Klingler, T. Wimmer, S. Geprägs, R. Gross, H. Huebl, and S. T. B. Goennenwein, Magnon-based logic in a multi-terminal YIG/Pt nanostructure, *Appl. Phys. Lett.* **109**, 022405 (2016).
- [20] S. Klingler, P. Pirro, T. Brächer, B. Leven, B. Hillebrands, and A. V. Chumak, Spin-wave logic devices based on isotropic forward volume magnetostatic waves, *Appl. Phys. Lett.* **106**, 212406 (2015).
- [21] B. Z. Rameshti, S. V. Kusminskiy, J. A. Haigh, K. Usami, D. Lachance-Quirion, Y. Nakamura, C.-M. Hu, H. X. Tang, G. E. W. Bauer, and Y. M. Blanter, Cavity magnonics, *Phys. Rep.* **979**, 1 (2022).
- [22] Y. Tabuchi, S. Ishino, A. Noguchi, T. Ishikawa, R. Yamazaki, K. Usami, and Y. Nakamura, Coherent coupling between a ferromagnetic magnon and a superconducting qubit, *Science* **349**, 405 (2015).
- [23] D. Lachance-Quirion, S. P. Wolski, Y. Tabuchi, S. Kono, K. Usami, and Y. Nakamura, Entanglement-based single-shot detection of a single magnon with a superconducting qubit, *Science* **367**, 425 (2020).
- [24] A. Chumak, P. Kabos, M. Wu, C. Abert, C. Adelmann, A. O. Adeyeye, J. Åkerman, F. G. Aliev, A. Anane, A. Awad, and C. H. Back, Advances in magnetics roadmap on spin-wave computing, *IEEE Trans. Magn.* **58**, 0800172 (2022).
- [25] P. Pirro, V. I. Vasyuchka, A. A. Serga, and B. Hillebrands, Advances in coherent magnonics, *Nat. Rev. Mater.* **6**, 1114 (2021).
- [26] A. Barman, G. Gubbiotti, S. Ladak, A. O. Adeyeye, M. Krawczyk, J. Gräfe, C. Adelmann, S. Cotofana, A. Naeemi, and V. I. Vasyuchka, *et al.*, The 2021 magnonics roadmap, *J. Phys.: Condens. Matter* **33**, 413001 (2021).
- [27] A. V. Chumak, V. I. Vasyuchka, A. A. Serga, and B. Hillebrands, Magnon spintronics, *Nat. Phys.* **11**, 453 (2015).
- [28] B. Lenk, H. Ulrichs, and F. G. M. Munzenberg, The building blocks of magnonics, *Phys. Rep.* **507**, 107 (2011).
- [29] G. Csaba, A. Papp, and W. Porod, Perspectives of using spin waves for computing and signal processing, *Phys. Lett. A* **381**, 1471 (2017).
- [30] A. A. Serga, A. V. Chumak, and B. Hillebrands, YIG magnonics, *J. Phys. D: Appl. Phys.* **43**, 264002 (2010).
- [31] V. V. Kruglyak, S. O. Demokritov, and D. Grundler, Magnonics, *J. Phys. D: Appl. Phys.* **43**, 264001 (2010).
- [32] O. V. Dobrovolskiy, R. Sachser, T. Bracher, T. Fischer, V. V. Kruglyak, R. V. Vovk, V. A. Shklovskij, M. Huth, B. Hillebrands, and A. V. Chumak, Magnon-fluxon interaction in a ferromagnet/superconductor heterostructure, *Nat. Phys.* **15**, 477 (2019).
- [33] O. V. Dobrovolskiy, Q. Wang, D. Y. Vodolazov, B. Budinska, R. Sachser, A. V. Chumak, M. Huth, and A. I. Buzdin, Cherenkov radiation of spin waves by ultra-fast moving magnetic flux quanta, (2021), [ArXiv:2103.10156](https://arxiv.org/abs/2103.10156).
- [34] I. A. Golovchanskiy, N. N. Abramov, V. S. Stolyarov, V. V. Bolginov, V. V. Ryazanov, A. A. Golubov, and A. V. Ustinov, Ferromagnet/superconductor hybridization for magnonic applications, *Adv. Funct. Mater.* **28**, 1802375 (2018).
- [35] I. A. Golovchanskiy, N. N. Abramov, V. S. Stolyarov, V. V. Ryazanov, A. A. Golubov, and A. V. Ustinov, Modified dispersion law for spin waves coupled to a superconductor, *J. Appl. Phys.* **124**, 233903 (2018).
- [36] I. A. Golovchanskiy, N. N. Abramov, V. S. Stolyarov, P. S. Dzhumaev, O. V. Emelyanova, A. A. Golubov, V. V. Ryazanov, and A. V. Ustinov, Ferromagnet/superconductor hybrid magnonic metamaterials, *Adv. Sci.* **6**, 1900435 (2019).
- [37] T. Yu and G. E. W. Bauer, Efficient Gating of Magnons by Proximity Superconductors, *Phys. Rev. Lett.* **129**, 117201 (2022).
- [38] I. A. Golovchanskiy, N. N. Abramov, V. S. Stolyarov, M. Weides, V. V. Ryazanov, A. A. Golubov, A. V. Ustinov, and M. Y. Kupriyanov, Ultrastrong photon-to-magnon coupling in multilayered heterostructures involving superconducting coherence via ferromagnetic layers, *Sci. Adv.* **7**, eabe8638 (2021).
- [39] I. A. Golovchanskiy, N. N. Abramov, V. S. Stolyarov, A. A. Golubov, M. Y. Kupriyanov, V. V. Ryazanov, and A. V. Ustinov, Approaching Deep-Strong On-Chip Photon-to-Magnon Coupling, *Phys. Rev. Appl.* **16**, 034029 (2021).
- [40] L.-L. Li, Y.-L. Zhao, X.-X. Zhang, and Y. Sun, Possible evidence for spin-transfer torque induced by spin-triplet supercurrents, *Chin. Phys. Lett.* **35**, 077401 (2018).
- [41] K.-R. Jeon, C. Ciccarelli, H. Kurebayashi, L. F. Cohen, X. Montiel, M. Eschrig, T. Wagner, S. Komori, A. Srivastava, J. W. Robinson, and M. G. Blamire, Effect of Meissner Screening and Trapped Magnetic Flux on Magnetization Dynamics in Thick Nb/Ni₈₀Fe₂₀/Nb Trilayers, *Phys. Rev. Appl.* **11**, 014061 (2019).
- [42] I. A. Golovchanskiy, N. N. Abramov, V. S. Stolyarov, V. I. Chichkov, M. Silaev, I. V. Shchetinin, A. A. Golubov, V. V. Ryazanov, A. V. Ustinov, and M. Y. Kupriyanov, Magnetization Dynamics in Proximity-Coupled Superconductor-Ferromagnet-Superconductor Multilayers, *Phys. Rev. Appl.* **14**, 024086 (2020).
- [43] S. V. Mironov and A. I. Buzdin, Giant demagnetization effects induced by superconducting films, *Appl. Phys. Lett.* **119**, 102601 (2021).
- [44] M. A. Silaev, Anderson-Higgs Mass of Magnons in Superconductor/Ferromagnet/Superconductor Systems, *Phys. Rev. Appl.* **18**, L061004 (2022).

- [45] I. Neudecker, G. Woltersdorf, B. Heinrich, T. Okuno, G. Gubbiotti, and C. Back, Comparison of frequency, field, and time domain ferromagnetic resonance methods, *J. Magn. Magn. Mat.* **307**, 148 (2006).
- [46] S. S. Kalarickal, P. Krivosik, M. Wu, C. E. Patton, M. L. Schneider, P. Kabos, T. J. Silva, and J. P. Nibarger, Ferromagnetic resonance linewidth in metallic thin films: Comparison of measurement methods, *J. Appl. Phys.* **99**, 093909 (2006).
- [47] Y.-C. Chen, D.-S. Hung, Y.-D. Yao, S.-F. Lee, H.-P. Ji, and C. Yu, Ferromagnetic resonance study of thickness-dependent magnetization precession in Ni₈₀Fe₂₀ films, *J. Appl. Phys.* **101**, 09C104 (2007).
- [48] I. A. Golovchanskiy, V. V. Bolginov, N. N. Abramov, V. S. Stolyarov, A. B. Hamida, V. I. Chichkov, D. Roditchev, and V. V. Ryazanov, Magnetization dynamics in dilute Pd_{1-x}Fe_x thin films and patterned microstructures considered for superconducting electronics, *J. Appl. Phys.* **120**, 163902 (2016).
- [49] D. Stancil, *Theory of Magnetostatic Waves* (Springer-Verlag New York, Inc., New York, 1993).
- [50] A. I. Gubin, K. S. Ilin, S. A. Vitusevich, M. Siegel, and N. Klein, Dependence of magnetic penetration depth on the thickness of superconducting Nb thin films, *Phys. Rev. B* **71**, 064503 (2005).
- [51] M. Houzet, Ferromagnetic Josephson Junction with Precessing Magnetization, *Phys. Rev. Lett.* **101**, 057009 (2008).
- [52] M. Tinkham, *Introduction to Superconductivity* (Courier Corporation, New York, 1996).
- [53] A. J. Annunziata, D. F. Santavicca, L. Frunzio, G. Catelani, M. J. Rooks, A. Frydman, and D. E. Prober, Tunable superconducting nanoinductors, *Nanotechnol.* **21**, 445202 (2010).
- [54] C. Kittel, Excitation of spin waves in a ferromagnet by a uniform rf field, *Phys. Rev.* **100**, 1295 (1958).
- [55] M. H. Seavey and P. E. Tannenwald, Direct observation of spin wave resonance, *J. Appl. Phys.* **30**, S227 (1959).
- [56] M. Sparks, Ferromagnetic resonance in thin films. I. Theory of normal-mode frequencies, *Phys. Rev. B* **1**, 3831 (1970).
- [57] S. Klingler, A. V. Chumak, T. Mewes, B. Khodadadi, C. Mewes, C. D. O. S. B. Hillebrands, and A. Conca, Measurements of the exchange stiffness of YIG films using broadband ferromagnetic resonance techniques, *J. Phys. D: Appl. Phys.* **48**, 015001 (2015).
- [58] I. A. Golovchanskiy, I. V. Yanilkin, A. I. Gumarov, B. F. Gabbasov, N. N. Abramov, R. V. Yusupov, R. I. Khaibullin, and L. R. Tagirov, Exchange spin waves in thin films with gradient composition, *Phys. Rev. Mater.* **6**, 064406 (2022).
- [59] C. H. Bajorek and C. H. Wilts, Evidence for partial surface spin pinning in ferromagnetic resonance, *J. Appl. Phys.* **42**, 4324 (1971).
- [60] H. PuszkarSKI, Theory of surface states in spin wave resonance, *Prog. Surf. Sci.* **9**, 191 (1979).